Journal of Materials Science: Materials in Electronics 34 (2023), p. 1201/1-11
https://doi.org/10.1007/s10854-023-10628-y

The effects of hydrogenation on the properties of heavy ion irradiated β-Ga_2O_3

A.Y. Polyakov[1], A. Kuznetsov[2], A. Azarov[2], A.V. Miakonkikh [3], A.V. Chernykh[1], A.A. Vasilev[1], I.V. Shchemerov[1], A.I. Kochkova[1], N. R. Matros[1] and S.J. Pearton[4*]

[1.] National University of Science and Technology MISiS, 4 Leninsky Avenue, Moscow 119049,

[2]Department of Physics/ Centre for Materials Science and Nanotechnology, University of Oslo, Problemveien 7, 0315 Oslo, Norway

[3]Valiev Institute of Physics and Technology, Russian Academy of Sciences (Valiev IPT RAS), Moscow, 117218, Nahimovsky Ave, 36(1), Russia

[4.] Department of Materials Science and Engineering, University of Florida, Gainesville, FL 32611, USA

*Corresponding author: E-mail: spear@ mse.ufl.edu

ABSTRACT

Defects created in lightly doped (2×10^{16} cm^{-3}) (010)-oriented bulk β-Ga_2O_3 implanted with 1.2 MeV, 3×10^{15} cm^{-2} $^{197}Au^{+}$ ions before and after treatment in hydrogen plasmas at 330^{o}C were studied by x-ray measurements, Rutherford backscattering spectra, capacitance-voltage, current-voltage, admittance spectra and deep level transient spectroscopy. Au implantation creates defects that produce total depletion of carriers in the top 1.5 μm and introduces electron traps with energy levels at E_c-0.7 eV, E_c-1.05 eV, E_c-0.45 eV, and deep acceptors with optical ionization thresholds near 1.3 eV, 2.3 eV and 3.1 eV, similar to the centers dominating the spectra of deep traps in β-Ga_2O_3. Hydrogen plasma treatment greatly enhances the photocurrent and photo-capacitance and decreases the width of the insulating layer produced by Au implantation. The results can be explained by hydrogen passivation of the triply charged Ga vacancies and doubly charged split Ga vacancies acceptors in the implanted region, returning part of this region to n-type conductivity.

Journal of Materials Science: Materials in Electronics 34 (2023), p. 1201/1-11
https://doi.org/10.1007/s10854-023-10628-y

I.INTRODUCTION

Studies of the effects of swift heavy ions on the structural and electronic properties of β-Ga_2O_3 semiconductor are of interest because this material is under development for next generation power electronic devices and solar-blind far-UV photodetectors [1-3]. One of the important considerations for new materials system for use in practical devices is their radiation tolerance, an indication of their lifetime when subjected to irradiation with high energy particles. Such studies have been carried out for β -Ga_2O_3 crystals, films, heterojunctions and devices for electrons, protons, α-particles, neutrons and γ-rays to assess suitability for systems employed in military applications, nuclear power production, avionics and space applications [4-6]. The radiation tolerance of β-Ga_2O_3 appears to be on a par with GaN or SiC. Given the projected superior performance of Ga_2O_3 devices due to higher electric breakdown field and bandgap, this is another positive aspect of the technology. However, in applications in avionics and particularly deep space, the damage produced by high energy heavy particles present in the cosmic ray flux becomes a concern [6]. For GaN and SiC, much is already known [6].

For β-Ga_2O_3 these studies are at an early stage, and have focused on changes in electrical performance of β-Ga_2O_3 Schottky diodes and solar-blind photodetectors and on monitoring structural changes occurring upon irradiation with heavy particles, such as 5-10 MeV ^{181}Ta or ^{86}Kr [7], 16 MeV Ta [8], 2096 MeV ^{181}Ta [9], 100 MeV Ag^{7+} [10], 120 MeV Au^{9+} [11] and 946 MeV Au [12]. These results point to increases in ideality factor and leakage current of Schottky diodes [7-12], changes in effective donor concentrations with high carrier removal rates > 10^6 cm^{-1} [9], decrease of photosensitivity and increase of photocurrent decay time [10]. Structural studies using Transmission Electron Microscopy (TEM) point to a prominent role of amorphous tracks along the ion paths explained by local melting and re-solidification of material [12], described by an inelastic thermal spike model [13]. The parameters degradation by high energy heavy particles are more pronounced than for SiC and GaN, in part due to the larger diameter of the spikes occasioned by the low thermal conductance of Ga_2O_3 and its higher bandgap resulting

in lower losses going into the electronic system and thus a decreased efficiency of dynamic annealing [6,10, 11], [10].

For β-Ga_2O_3 implanted with high fluences of ions (Si, Sn, Ni, Ga, Au, Ar), an additional concern is that, instead of amorphization that is common for many semiconductors, β-Ga_2O_3 undergoes a structural transformation in the implanted region upon such high-dose implantations. There remains debate on the nature of this structural transition. Anber et al. [14] assigned the modified structure in implanted β-Ga_2O_3 to the formation of orthorhombic κ-Ga_2O_3 polymorph that is metastable and turns into stable monoclinic β-Ga_2O_3 upon heating to 700-800^{o}C [1, 2]. This attribution is supported by Azarov et al. [15] on the strength of their analysis of XRD, STEM, RBS studies of β-Ga_2O_3 implanted with high doses of Ni, Ga, Au. This phase change was attributed to the high strain accumulated in heavily irradiated β-Ga_2O_3 driving the formation energy of implanted κ-Ga_2O_3 below that of β-Ga_2O_3. On the other hand, Garcia-Fernandes et al [16] interpreted the STEM patterns in the implanted region of β-Ga_2O_3 to the formation of another metastable polymorph of Ga oxide, γ-Ga_2O_3 with the structure of defect spinel. Yoo et al. [17] studying the STEM images of heavily Sn implanted β-Ga_2O_3 came to the same conclusions. They observed the structure in the implanted layer to revert to β-Ga_2O_3 after annealing to 1100^{o}C, but the thin layer on top still staying in the form of γ-Ga_2O_3. It was suggested [18] that the interplay between strain and disorder gives rise to an additional degree of freedom and regulates formation of the predominant polymorph. Finally, Petkov et al. [19] were able to interpret the structure forming in β-Ga_2O_3 upon in-situ Ar irradiation as arising from severely deformed β-Ga_2O_3.

Resolving this is important because the κ-Ga_2O_3 phase is reported to possess very high spontaneous polarization and prominent ferroelectric properties [20-22], which could be employed in field effect transistors with polarization doping [21] by ion implantation if the implanted β-Ga_2O_3 could be rendered conducting without destroying the κ-Ga_2O_3 polymorph [15].

Journal of Materials Science: Materials in Electronics 34 (2023), p. 1201/1-11
https://doi.org/10.1007/s10854-023-10628-y

Previously we attempted to achieve that by implanting semi-insulating β-Ga_2O_3(Fe) with Ga and Si [23]. The films in the as-implanted state were highly resistive, and implantation with Si with subsequent annealing to temperatures compatible with preserving the potential κ-Ga_2O_3 polymorph intact (up to 600^{o}C) failed to activate n-type conductivity. However, treating the samples in a hydrogen plasma at 330^{o}C rendered the implanted layer n-type, albeit with a low net donor concentration of 10^{12}-10^{13} cm^{-3}. The higher end of this range was achieved with lower implantation temperatures for the Si. This was attributed to formation of shallow donor complexes with hydrogen by radiation defects, presumably Ga vacancies which occur in β-Ga_2O_3 annealed in molecular hydrogen [24] or treated in hydrogen plasmas at moderate temperatures [25]. The same mechanism has been invoked to explain changes of electrical properties of β-Ga_2O_3 implanted with oxygen ions and treated in hydrogen plasmas [26].

In this paper, we describe electrical characterization of lightly n-type doped bulk β-Ga_2O_3 implanted with 1.2 MeV $^{197}Au^+$ ions before and after the treatment in H plasma and compare these results with previous observations for implanted and H plasma treated β-Ga_2O_3 crystals.

II.EXPERIMENTAL

The samples used for Au implantation studies were (010)-oriented bulk β-Ga_2O_3 unintentionally doped n-type crystal having net donor density below 10^{17} cm^{-3} [27]. These were implanted with 1.2 MeV $^{197}Au^+$ ions to fluence of 3×10^{15} cm^{-2}. Structural characterization involved x-ray measurements in θ–2θ mode and Rutherford Backscattering Spectrometry in channeling mode (RBS/C) [15]. For electrical characterization, Ti/Au Ohmic (20 nm/80 nm) contacts were deposited on the back surface of the samples and circular semi-transparent Ni Schottky diodes of 1 mm diameter and 20 nm thickness deposited on the front surface after implantation. Contact preparations were done after implantation using e-beam sputtered. Schottky diodes deposited via a shadow mask.

Electrical characterization involved current-voltage (I-V) measurements in the dark and under illumination with high-power Light Emitting Diodes (LEDs) with peak photon energies ranging from 1.3 eV to 4.8 eV, capacitance versus frequency (C-f) and capacitance versus voltage (C-V) measurements in the dark and under monochromatic illumination with the same set of LEDs as used in I-V measurements. The output optical power density used in these experiments was 250 mW/cm^2 for LEDs with photon energies from 1.3 eV to 3.4 eV, 15 mW/cm^2 for the LED with peak photon energy 4.5 eV, and 1.2 mW/cm^2 for the LED with peak photon energy 4.8 eV. The results of C-f and C-V measurements under illumination were used to characterize the optical ionization energies and concentrations of deep traps below the Fermi level using Light Capacitance Voltage (LCV) [28]. In addition, the samples were characterized by current versus temperature (I-T) measurements performed upon cooling down in the dark and after illumination. These allowed determination of the Fermi level pinning position in the dark and to characterize the deep centers capable of trapping electrons or holes and giving rise to features in Thermally Stimulated Current (TSC) spectra [29]. These were complemented by Admittance Spectra (AS) [30], Deep Level Transient Spectroscopy with electron injection (DLTS) and with optical injection (ODLTS) [30], and by Photoinduced Current Transient Spectroscopy (PICTS) [31]. Experimental setups were described previously [32-34]. The implanted samples were also exposed to a hydrogen plasma at 330^{o}C for 0.5 hours [23, 25, 26].

III. RESULTS AND DISCUSSION

We begin with XRD and RBS/C measurements before and after implantation with Au. Fig. 1(a) displays the θ–2θ XRD patterns in the vicinity of the β-Ga_2O_3 (020) reflection. Implantation gives rise to an additional broad peak located between the Bragg angles of 63.5^o and 63.8^o and strong broadening of the β-Ga_2O_3 (020) peak towards higher Bragg angles. In RBS/C spectra (Fig. 1(b)) one observes a box-like increase of the yield for the near surface region with the damage peaked near the depth of 350 nm (red line). The yield near the peak is

~80% of the signal calculated for random scattering expected for a fully disordered amorphous sample [15] (olive line).

Fig 2(a) presents the Au implantation profile and the defect (represented by vacancies) profile calculated by using the Stopping and Range Ions in Matter (SRIM) package [35]. As discussed in Ref. [36], for heavy ions, such as Au, particularly for the propagation in the targets containing light atoms, such as Ga_2O_3, the full cascade version of the model has to be employed in order to obtain realistic relations between the nuclear and electronic losses and to produce realistic distributions of damage as represented by generated vacancies. Otherwise, the contribution of electronic losses is considerably overestimated and the peak of distribution of implantation damage is shifted towards the surface and in general tends to be located near to the calculated range of ions. Fig. 2(b) presents the dependence of calculated electronic and nuclear losses as a function of Au ions energy and shows that, for the Au energy of 1.2 MeV, the nuclear losses far exceed the electronic losses. The range of Au ions is thus predicted to be close to 300 nm with the peak of distribution lying at 200 nm. The defect concentration distribution shows another peak near 400 nm and a long tail extending far inside the sample (Fig. 2(a)). This correlates with the RBS/C spectrum in Fig. 1(b). There will also be defects extending deeper into the sample , resulting from enhanced diffusion under ionization.

The electrical measurements indicate the lattice damage extends deeper than estimated by RBS/C data in Fig. 1(b) and even deeper than predicted by SRIM modeling in Fig. 2(a). Fig. 3(a) shows the room temperature C-f dependence for the implanted sample measured at 0V. The capacitance on the frequency plateau is 45 pF. This means the implanted sample is depleted of mobile charge carriers to 1.5 μm, which suggests the presence of a highly resistive region of that thickness. The structure behaves as Metal-Insulator-Semiconductor (MIS) [30], with the heavily damaged region playing the role of insulator. The C-V profiling gives the charge distribution for three different temperatures in Fig. 4(a). At large distances from the boundary with the implanted region, the charge concentration shows a plateau corresponding to the net donor density in the

substrate. Closer to the interface, the charge concentration displays a depletion due to the existence of a barrier between the highly resistive damaged region and the bulk of the sample not affected by Au implantation.

The changes in C-f characteristics produced by illumination are illustrated by Figure S1(a) of the Supplementary Material. The photo-capacitance normalized by the dark capacitance is presented in Fig. 3(b). This shows optical thresholds near 1.3 eV, 2 eV, 3 eV. Measurements of charge concentration profile occurring under illumination (Fig. 4(b)) indicate the main changes induced by illumination occur near the boundary with the undamaged layer where the density of radiation defects is the lowest. Closer to the surface where the density of defects is high, the photogenerated carriers are rapidly re-trapped and do not contribute to photo-capacitance.
The dark current was very low at reverse bias and at forward bias for forward voltage below 1.5 V when it strongly increased showing the current growing with voltage as V^2, likely related to Trap Limited Current (TLC) mode [37] coming into play when efficient electrons injection from the Schottky metal and from the undamaged n-region of the sample became dominant, although the details of the process still need to be understood. The dependence of current on photon energy is shown in Fig. S3(a) of the Supplementary Material, while the actual reverse photocurrent spectrum is presented in Fig. 5(a). The optical thresholds observed in photocurrent are similar to those seen in photocapacitance.

Admittance spectra showed a prominent step in capacitance (Fig. S2(a)) Supplementary Material) [30] and an activation energy of the dominant center of 0.71 eV with electron capture cross section of 8.5×10^{-15} cm^2 (see Fig. 6(a)).

In DLTS measurements, the application of the forward bias pulse fills the traps near the interface between the damaged implanted region and the undamaged region with electrons and detects emission from these traps in subsequent capacitance relaxations monitored by DLTS. When the applied reverse bias is high so that the space charge region boundary is located in the undamaged region and remains there with applied filling pulse of low negative value, one can

detect the deep electron traps coming from the undamaged substrate. The spectrum is shown in Fig. 7, corresponding to the reverse bias -2V and forward bias pulse of 1V probing the edge of the damaged region. The centers seen have ionization energy 0.45 eV (electron capture cross section $\sigma_n=3\times10^{-15}$ cm^2), 0.73 eV ($\sigma_n=1.1\times10^{-14}$ cm^2), and 1.05 eV ($\sigma_n=1.3\times10^{-13}$ cm^2). These three traps are like the well-known centers in β-Ga_2O_3, E2* (E_c-0.73-0.75 eV), E3 (E_c-1.05 eV). These are known to be prominent radiation defects related to native defects or their complexes [5] and centers E_c-0.45 eV observed in β-Ga_2O_3 [25] related to the E1 centers [25]. This is supported by the DLTS spectra in the "bulk" undamaged portion probed with reverse bias of -5V and forward bias pulse of -2V. The spectra of the damaged and undamaged portions of the sample are compared in Fig. S4 of the Supplementary Material) that indicates the density of E2* is greatly enhanced in the damaged region.

In ODLTS with optical excitation (Fig. 8(a)) taken with 4.5 eV(277 nm wavelength) LED excitation at reverse bias of -1V, the peaks coming from the electron traps are superimposed on a wide hole-trap-like structureless band (the convention in all DLTS figures in this work is that the peaks caused by electron traps (i.e. traps that cause the capacitance after the injection pulse increase with time [30]) are positive, and the peaks due to hole trapping are negative).

Hydrogen plasma treatment at 330^{o}C gave rise to several changes. The capacitance at 0V became higher, 55 pF as compared to 45 pF in Fig. 3(a) meaning the fully depleted damaged region became thinner, 1.1 μm instead of 1.5 μm. This is illustrated by the results of C-V profiling in Fig. 4(c)). The photocapacitance signal became stronger (the C-f characteristics measured at 0V with illumination with different photon energies are shown in Fig. S2(b) of the complementary material, while the photo-capacitance spectrum is presented in Fig. 3(b)). From comparing the photo-capacitance spectra before and after H plasma treatment, the major optical thresholds in the spectra are not changed, but the magnitude of the steps in photo-capacitance due to centers with optical ionization threshold 2 eV and 3.1 eV are increased.

In admittance spectra (Fig. 6(b) and Fig. S2(b) in the Supplementary Material), both the amplitude of capacitance steps and the magnitude of the high temperature peak in dC/dT spectrum have increased and an additional step in capacitance and peak in dC/dT that correspond to the trap with activation energy 0.45 eV (σ_n=6.7×10^{-15} cm^2) appeared. The photocurrent became much higher, implying strong suppression of recombination of charge carriers in the damaged region (the I-V characteristics measured under illumination are shown in Fig. S3(b) of the Supplementary Material, while the photocurrent spectra before and after H plasma treatment are compared in Fig. 5).

However, in DLTS spectra of the damaged region taken with applied bias -2V and forward bias pulse of 1V, one observes an increase of the E2*, E3 electron traps and the E_c-0.45 eV center (E1-like trap [25]). The ODLTS spectra after H plasma treatment were dominated by the E_c-0.45 eV (E1-like), E_c-0.7 eV (E2*), E_c-1.05 eV (E3) traps, with the hole-trap-like signal suppressed (Fig. 7).

The deep traps detected before and after H plasma treatment are similar to the centers detected in proton irradiated β-Ga_2O_3 [5] and in O implanted and H plasma treated β-Ga_2O_3 [26].

This suggests that the damaged region, at least in its peripheral portion adjacent to the unaffected part of the crystal, is still β-Ga_2O_3, but having a high density of radiation defects. If this is the case, a possible scenario explaining the results after the Au implantation and subsequent H plasma treatment would be that the portion of the sample adjacent to the boundary of the damaged region consists of triply charged Ga vacancies V_{Ga}^{3-} responsible for the 3.1 eV band in photo-capacitance [5] and of doubly charged split Ga vacancies V_{Ga}^{i2-} believed to be associated with the 2 eV photo-capacitance band [38]. In addition, deep electron traps E2*, E3*, E1 due to native defects [5] are present. H plasma treatment partly passivates the V_{Ga}^{3-} and the V_{Ga}^{i2}-compensating acceptors, rendering the periphery of the damaged crystal conducting and effectively decreasing the width of the fully depleted region. The DLTS, ODLTS, AS, photo-

capacitance and photocurrent measurements in such samples are probing the part of the Au implanted crystal closer to the surface than before the hydrogen plasma treatment. The density of all defects in this region is higher, which is manifested in the enhanced DLTS/ODLTS features due to electron traps, and in photo-capacitance spectra showing enhanced V_{Ga} and V_{Ga}^{i} features. Very roughly the concentrations of defects in the peripheral region probed by DLTS and Steady-State Photocapacitance (SSPC) can be estimated for electron traps from the height of DC/C peaks in DLTS as $2N_d\Delta C/C$ (see Fig. 7) if one does not account for the λ-correction [30] and assumes the donors concentration to be the one calculated in C-V profiling in Fig. 4, for hole traps in SSPC spectra the concentrations can be estimated from $2N_d\Delta C_{ph}/C_{dark}$ in Fig. 3. The results are presented in Table I.

Hydrogen passivates the deep centers in the Au implanted layer that are lifetime killers. In the simplest case, they could be due to Au acceptors in β-Ga_2O_3.

CONCLUSIONS

Implantation of lightly n-type bulk β-Ga_2O_3 with Au ions of the energy of 1.2 MeV and the fluence of 3×10^{15} cm^{-2} renders the top 1.5 μm highly resistive. The thickness of this layer is higher than the estimated projected range of Au, which could be related to diffusion of primary defects. The region adjacent to the boundary of this high resistivity layer and the undamaged crystal is characterized by an increased density of deep electron traps at E_c-0.73 eV, E_c-1.05 eV, and E_c-0.45 eV, like the radiation defects E2*, E3, E1 commonly observed in β-Ga_2O_3. This suggests that the damaged region, at least in its peripheral portion adjacent to the unaffected part of the crystal, is still β-Ga_2O_3, albeit with a high density of defects. Recent work of Azarov et al [39] who have shown that the combination of γ-Ga_2O_3/β-Ga_2O_3 is the reason for the exceptional radiation tolerance of β-Ga_2O_3 that does not become amorphous even when subjected to extremely high doses of implantation seems to support such an explanation. Treatment of the Au implanted samples in hydrogen plasma at 330°C decreased the width of the high resistivity layer, increased the density of the E2*, E3, E1 electron traps, increased the overall photo-capacitance

and photocurrent and increased the contribution of the traps with optical ionization thresholds 2 eV and 3.1 eV. It also increased the photosensitivity in the near band edge region.

The results can be qualitatively explained by assuming that the hydrogen passivates the triply charged Ga vacancies and doubly charged split Ga vacancies acceptors in the peripheral region, returning part of this region to n-type conductivity. It also partly passivates the major lifetime killer in the implanted film, thus increasing the photosensitivity.

ACKNOWLEDGMENTS

The work at NUST MISiS was supported in part by a grant from the Ministry of Science and Higher Education of Russian Federation (Agreement # 075-15-2022-1113). The international collaboration was enabled by the INTPART program at the Research Council of Norway via project No. 322382. The work at UF was funded by the Defense Threat Reduction Agency (DTRA) as part of the Interaction of Ionizing Radiation with Matter University Research Alliance (IIRM-URA) under contract number HDTRA1-20-2-0002. The content of the information does not necessarily reflect the position or the policy of the federal government, and no official endorsement should be inferred. The work at UF was also supported by NSF DMR 1856662.

Journal of Materials Science: Materials in Electronics 34 (2023), p. 1201/1-11
https://doi.org/10.1007/s10854-023-10628-y

References

[1] S. J. Pearton, Fan Ren, Marko Tadjer and Jihyun Kim, Perspective: Ga_2O_3 for ultra-high power rectifiers and MOSFETS, J. Appl. Phys. 124, 220901 (2018).

[2] Gallium Oxide: Materials Properties, Crystal Growth, and Devices, ed. Masataka Higashiwaki and Shizuo Fujita (Springer Series in Materials Science ISBN 978-3-030-37152-4 ISBN 978-3-030-37153-1, 2020)

[3] J. Xu, W. Zheng and F. Huang. Gallium oxide solar-blind ultraviolet photodetectors: a review. J. Mater. Chem. C, 7, 8753 (2019).

[4] J. Kim, S. J. Pearton, C. Fares, J. Yang, R. Fan, S. Kim, and A. Y. Polyakov, "Radiation damage effects in Ga2O3 materials and devices," J. Mater. Chem. C **7**, 10 (2018)

[5] Alexander Y. Polyakov,Vladimir I. Nikolaev, Eugene B. Yakimov, Fan Ren, Stephen J. Pearton, and Jihyun Kim, Deep level defect states in β-, α-, and ε-Ga_2O_3 crystals and films: Impact on device performance, J. Vac. Sci. Technol. A 40, 020804 (2022)

[6] S. J. Pearton, Assel Aitkaliyeva, Minghan Xian, Fan Ren, Ani Khachatrian, Adrian Ildefonso, Zahabul Islam, Md Abu Jafar Rasel, Aman Haque, A. Y. Polyakov, and Jihyun Kim, Radiation Damage in Wide and Ultra-Wide Bandgap Semiconductors, ECS J. Solid State Sci. Technol., 2021 10 055008

[7] Wensi Ai, Lijun Xu, Shuai Nan, Pengfei Zhai, Weixing Li, Zongzhen Li, Peipei Hu, Jian Zeng, Shengxia Zhang, Li Liu, Youmei Sun , and Jie Liu, Radiation damage in β-Ga_2O_3 induced by swift heavy ions, Japan J. Appl. Phys. 58, 120914 (2019).

[8] Mingzhuo Hua, Zhourui Xu, Xusheng Tian, Zhengxing Wang, Chunfu Zhang, Shenglei Zhao, Yachao Zhang, Jing Ning, Qian Feng, Jincheng Zhang and Yue Hao, Influence of Swift Heavy Ion Irradiation on Electrical Characteristics of β-Ga2O3 Schottky Barrier Diode, Semicond. Sci. Technol. in press https://doi.org/10.1088/1361-6641/acb45e

[9] Wen-Si Ai , Jie Liu , Qian Feng , Peng-Fei Zhai , Pei-Pei Hu , Jian Zeng , Sheng-Xia Zhang , Zong-Zhen Li , Li Liu , Xiao-Yu Yan , and You-Mei Sun, Degradation of β-Ga2O3 Schottky barrier diode under swift heavy ion irradiation, Chin. Phys. B Vol. 30, No. 5 (2021) 056110

[10] Damanpreet Kaur, Pargam Vashishtha, Saif Ahmad Khan, Pawan K. Kulriya, Govind Gupta, and Mukesh Kumar, Phase dependent radiation hardness and performance analysis of amorphous and polycrystalline Ga2O3 solar-blind photodetector against swift heavy ion irradiation, : J. Appl. Phys. 128, 065902 (2020); doi: 10.1063/5.0019786

[11] N. Manikanthababu , Hardhyan Sheoran, K. Prajna , S. A. Khan, K. Asokan, J. V. Vas, R. Medwal, B. K. Panigrahi, and R. Singh, In Situ Electrical Characteristics and Defect Dynamics Induced by Swift Heavy Ion Irradiation in Pt/PtOx/β-Ga2O3 Vertical Schottky Barrier Diodes, IEEE Trans. Electron. Dev. 69, 5996 (2022).

[12] C. L. Tracy, M. Lang, D. Severin, M. Bender, C. Trautmann, and R. C. Ewing, "Anisotropic expansion and amorphization of Ga2O3 irradiated with 946 MeV Au ions," Nucl. Instrum. Methods Phys. Res. B, 374, pp. 40–44 (2016).

[13] A. Meftah et al., "Track formation in SiO2 quartz and the thermal-spike mechanism," Phys. Rev. B, Condens. Matter, vol. 49, no. 18, pp. 12457–12463, May 1994]

[14] E. A. Anber, D. Foley, A. C. Lang, J. Nathaniel, J. L. Hart, M. J. Tadjer, K. D. Hobart, S. Pearton, and M. L. Taheri, "Structural transition and recovery of Ge implanted β-Ga_2O_3," Appl. Phys. Lett. 117, 152101 (2020)

[15] Alexander Azarov, Calliope Bazioti, Vishnukanthan Venkatachalapathy, Ponniah Vajeeston, Edouard Monakhov, and Andrej Kuznetsov, Disorder-Induced Ordering in Gallium Oxide Polymorphs, Phys. Rev. Lett. 128, 015704 (2022)

[16] J. Garcıa-Fernandez, S., B. Kjeldby, P. D. Nguyen, O. B. Karlsen, L. Vines, and Ø. Prytz, Formation of γ-Ga_2O_3 by ion implantation: Polymorphic phase transformation of β-Ga_2O_3, Appl. Phys. Lett. 121, 191601 (2022)

[17] Timothy Yoo, Xinyi Xia, Fan Ren, Alan Jacobs, Marko J. Tadjer, Stephen Pearton, and Honggyu Kim, "Atomic-scale characterization of structural damage and recovery in Sn ion-implanted β-Ga_2O_3", Appl. Phys. Lett. 121, 072111 (2022).

[18] Alexander Azarov, Vishnukanthan Venkatachalapathy, Platon Karaseov, Andrei Titov, Konstantin Karabeshkin, Andrei Struchkov and Andrej Kuznetsov, Interplay of the disorder and strain in gallium oxide. Sci Rep 12, 15366 (2022)

[19] Alexander Petkov, David Cherns, Wei-Ying Chen, Junliang Liu, John Blevins, Vincent Gambin, Meimei Li, Dong Liu, and Martin Kuball, Structural stability of β-Ga_2O_3 under ion irradiation, Appl. Phys. Lett. 121, 171903 (2022).

[20] A. Parisini, A. Bosio, V. Montedoro, A. Gorreri, A. Lamperti, M. Bosi,G. Garulli, S. Vantaggio, and R. Fornari, "Si and Sn doping of ε-Ga_2O_3 layers," APL Mater. 7, 031114 (2019).

[21] H. von Wenckstern, "Group-III sesquioxides: Growth, physical properties and devices," Adv. Electron. Mater. 3, 1600350 (2017)

[22] Francesco Mezzadri, Gianluca Calestani, Francesco Boschi, Davide Delmonte, Matteo Bosi, and Roberto Fornari, Crystal Structure and Ferroelectric Properties of ε-Ga2O3 Films Grown on (0001)-Sapphire, Inorg. Chem. xxx, DOI: 10.1021/acs.inorgchem.6b02244

[23] A. Y. Polyakov, A. I. Kochkova, A. Azarov, V. Venkatachalapathy, A. V. Miakonkikh, A. A. Vasilev, A. V. Chernykh, I. V. Shchemerov, A. A. Romanov, A. Kuznetsov, and S. J. Pearton, Tuning electrical properties in Ga_2O_3 polymorphs induced with ion beams, J. Appl. Phys. 133, 095701 (2023); doi: 10.1063/5.0133181

[24] M. M. Islam, M. O. Liedke, D. Winarski, M. Butterling, A. Wagner,P. Hosemann, Y. Wang, B. Uberuaga, and F. A. Selim, Chemical manipulation of hydrogen induced high p-type and n-type conductivity in Ga2O3, Sci. Rep. 10, 6134 (2020)

[25] A. Y. Polyakov, In-Hwan Lee, Andrew Miakonkikh , A. V. Chernykh , N. B. Smirnov , I. V.Shchemerov, A. I. Kochkova, A. A. Vasilev, and S. J. Pearton, Anisotropy of hydrogen plasma effects in bulk n-type β-Ga2O3, J. Appl. Phys. 127, 175702 (2020);

[26] A.Y. Polyakov, A.A. Vasilev, I.V. Shchemerov, A.V. Chernykh, I.V. Shetinin, E.V. Zhevnerov, A.I. Kochkova, P.B. Lagov, A.V. Miakonkikh , Yu.S. Pavlov, U.A. Kobets, In-Hwan Lee, A. Kuznetsov, S.J. Pearton, Conducting surface layers formed by hydrogenation of O-implanted β-Ga2O3, Journal of Alloys and Compounds 945 (2023) 169258

[27] www.tamura-ss.co.jp/en/products

[28] Esmat Farzana, Max F. Chaiken, Thomas E. Blue, Aaron R. Arehart , and Steven A. Ringel, Impact of deep level defects induced by high energy neutron radiation in -Ga2O3, APL Mater. 7, 022502 (2019).

[29] D.K. Schroder, Semiconductor material and device characterization (Wiley-Interscience, 3rd Edition, New York, 2006)

[30] Capacitance spectroscopy of semiconductors, ed. Jian V. Li and Giorgio Ferrari (Pan Stanford Publishing Pte Ltd, Singapore, 2018) 437 pp

[31] M. Tapiero, N. Benjelloun, J.P. Zielinger, S. El Hamd, and C. Noguet, Photoinduced current transient spectroscopy in high-resistivity bulk materials: instrumentation and methodology, J. Appl. Phys. 54(8) 4006 (1988)

[32] A. Y. Polyakov, N. B. Smirnov, I. V. Shchemerov, S. J. Pearton, Fan Ren, A. V. Chernykh, and A. I. Kochkova, Electrical properties of bulk semi-insulating β-Ga2O3 (Fe), Appl. Phys. Lett. 113, 142102 (2018)

[33] A. Y. Polyakov, N. B. Smirnov, I. V. Shchemerov, S. J. Pearton, F. Ren, A. V. Chernykh, P. B. Lagov, and T. V.Kulevoy, Hole traps and persistent photocapacitance in proton irradiated -Ga2O3 films doped with Si, APL Materials 6, 096102 (2018)

[34] Alexander Y. Polyakov, Nikolai B. Smirnov, In-Hwan Lee, and Stephen J. Pearton, Deep level transient spectroscopy in III-Nitrides: Decreasing the effects of series resistance, Journal of Vacuum Science & Technology B 33, 061203 (2015)

[35] J. F. Ziegler, M. D. Ziegler, and J. P. Biersack, “SRIM—the stopping and range of ions in matter (2010)”, Nucl. Instrum. Methods Phys. Res. B **268,** 1818 **(**2010).

[36] William J. Weber and Yanwen Zhang, Predicting damage production in monoatomic and multi-elemental targets using stopping and range of ions in matter code: Challenges and recommendations, Current Opinion Solid State Mater. Sci. 23 (2019) 100757

[37] Kwan C. Cao and Wei Hwang, Electrical Transport in Solids (Pergamon Press, Oxford, New York, Toronto, 1981) volume 1

[38] J. M. Johnson, Z. Chen, J. B. Varley, C. M. Jackson, E. Farzana, Z. Zhang, A. R. Arehart, H.-L. Huang, A. Genc, S. A. Ringel, C. G. Van de Walle, D. A. Muller, and J. Hwang, Phys. Rev. X **9**, 041027 (2019)

[39] Alexander Azarov, Javier García Fernández, Junlei Zhao, Flyura Djurabekova, He Huan, He Ru, Øystein Prytz, Lasse Vines, Umutcan Bektas, Paul Chekhonin, Nico Klingner, Gregor Hlawacek and Andrej Kuznetsov, Universal radiation tolerant semiconductor, https://arxiv.org/abs/2303.13114)

[40] *Ultrawide Bandgap β-Ga2O3 Semiconductor: Theory and Applications*, edited by James S. Speck and Esmat Farzana [AIP Publishing (online), Melville, New York, 2023],chapter 12, available at: https://doi.org/10.1063/9780735425033

Journal of Materials Science: Materials in Electronics 34 (2023), p. 1201/1-11
https://doi.org/10.1007/s10854-023-10628-y

Table I. Concentrations of defects detected in peripheral part of the damaged region of the 1.2 MeV $^{197}Au^{+}$ implanted sample (fluence 3×1015 cm^{-2}) before and after hydrogen plasma treatment at 330^{o}C as measured by DLTS or Steady-State Photocapacitance (SSPC)

Defect level	Method of detection	Concentration (cm^{-3})		Possible origin
		Before H plasma	After H plasma	
E_c-0.45 eV	DLTS	2.8×10^{13}	5.8×10^{13}	Common center in (010) bulk, radiation defect [4, 5, 40]
E_c-0.73 eV	DLTS	1.4×10^{15}	2×10^{15}	E2* center, radiation defect [4, 5, 40]
E_c-1.05 eV	DLTS	1.2×10^{14}	2.9×10^{14}	E3 center, radiation defect [4, 5, 40]
E_c-2 eV	SSPC	7.2×10^{15}	5.3×10^{16}	Split Ga vacancy [4, 5, 40]
E_c-3.1 eV	SSPC	2.7×10^{15}	1.4×10^{17}	Possibly Ga vacancy [4, 5]

Journal of Materials Science: Materials in Electronics 34 (2023), p. 1201/1-11
https://doi.org/10.1007/s10854-023-10628-y

Figure Captions

Fig. 1 (Color online) (a) X-ray pattern of as-grown β-Ga_2O_3 sample (blue line) and of $^{197}Au^+$ 1.2 MeV 3×10^{15} cm^{-2} implanted sample (red line); (b)RBS/C spectra of Au implanted sample (red line); also shown are the spectrum for the virgin sample (blue line) and the random scattering spectrum characteristic for the amorphous sample (olive line).

Fig. 2 (color online) (a) the depth distribution of implanted Au and of vacancies in Au implanted at 1.2 MeV energy, 3×10^{15} cm^{-2} fluence β-Ga_2O_3(010) sample; (b) the energy dependence of electronic and nuclear losses in β-Ga_2O_3 for Au implantation.

Fig. 3 (Color online) (a) Room temperature photo-capacitance at 0V bias for the Au implanted sample before H plasma treatment (blue line) and after such treatment (red line); (b) the photo-capacitance normalized by the dark capacitance spectra (the color coding same as in (a)).

Fig. 4. (Color online) (a) Concentration profiles after Au implantation for 3 measurement temperatures; (b) 140K concentration profiles measured in the dark and under illumination with two photon energies; (c) 300K concentration profiles before and after H plasma treatment.

Fig. 5 (Color online) Photocurrent density measured at 140K at -2V after Au implantation (blue line) and subsequent H plasma treatment (red line).

Fig. 6 (Color online) (a) dC/dT spectra for several measurement frequencies (20 Hz, 30 Hz, 50 Hz, 100 Hz, 200 Hz) with bias -0.2V before Au irradiation; (b) same after H plasma treatment.

Fig.7. (Color online) DLTS spectra measured at 10 kHz, -2V, forward bias pulse +1V (50 ms long), with time windows 350 ms/3500 ms (solid lines) and 3.5 s/ 35 s (dashed lines) after Au implantation (blue lines) and after subsequent H_2 plasma exposure at 330^{o}C for 0.5 h (red line).

Fig.8 (Color online) (a) ODLTS spectra measured for Au implanted sample with 4.5 eV photons excitation, bias pulse 1 s long, reverse bias of -1V with time windows of 350 ms/ 3500 ms (solid line) and 2.45 s/24.5 s (dashed line); (b) ODLTS spectra measured for Au implanted sample after subsequent hydrogen plasma treatment; excitation conditions, applied bias and time windows are the same as in (a); for comparison the spectra of a Au implanted sample is also displaye

Journal of Materials Science: Materials in Electronics 34 (2023), p. 1201/1-11
https://doi.org/10.1007/s10854-023-10628-y

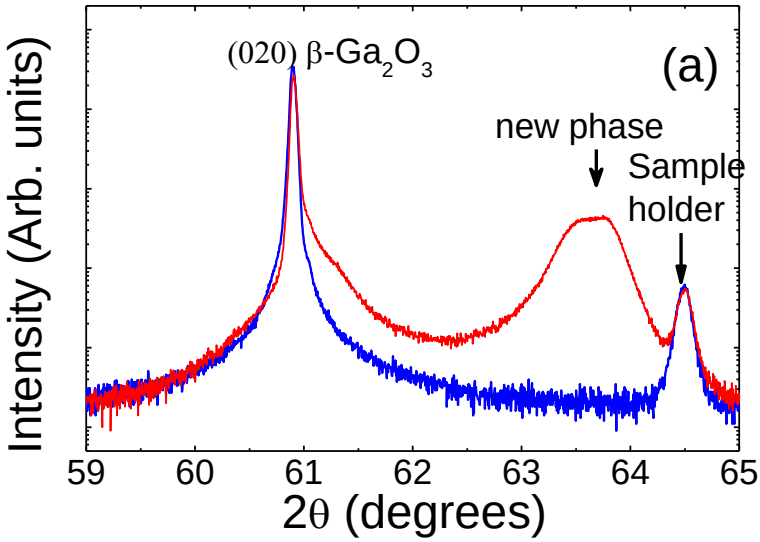

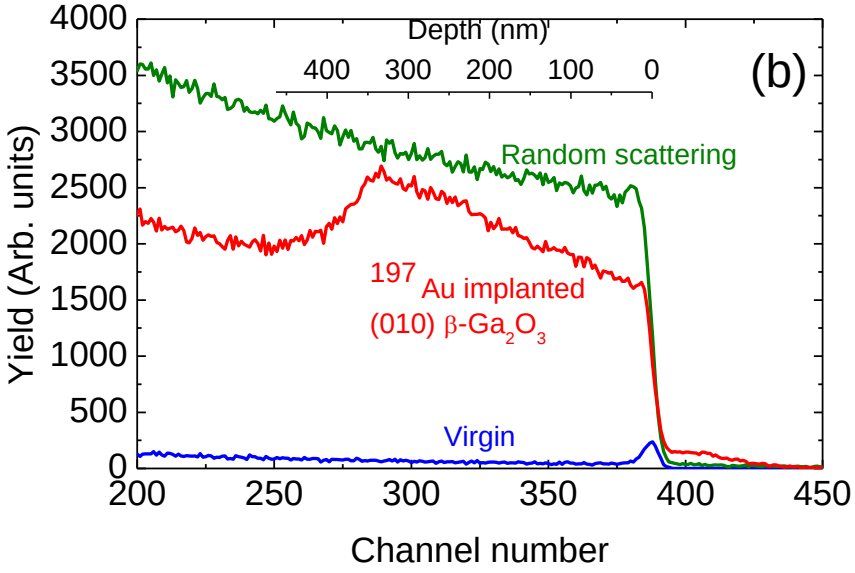

Journal of Materials Science: Materials in Electronics 34 (2023), p. 1201/1-11
https://doi.org/10.1007/s10854-023-10628-y

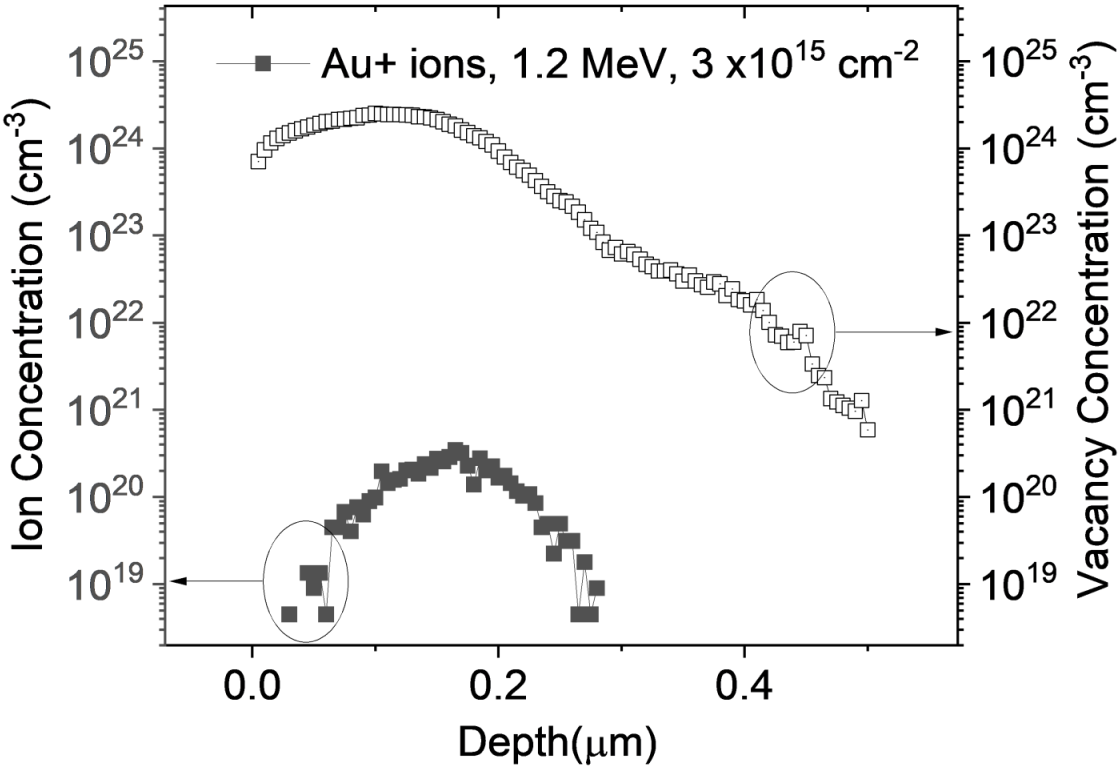

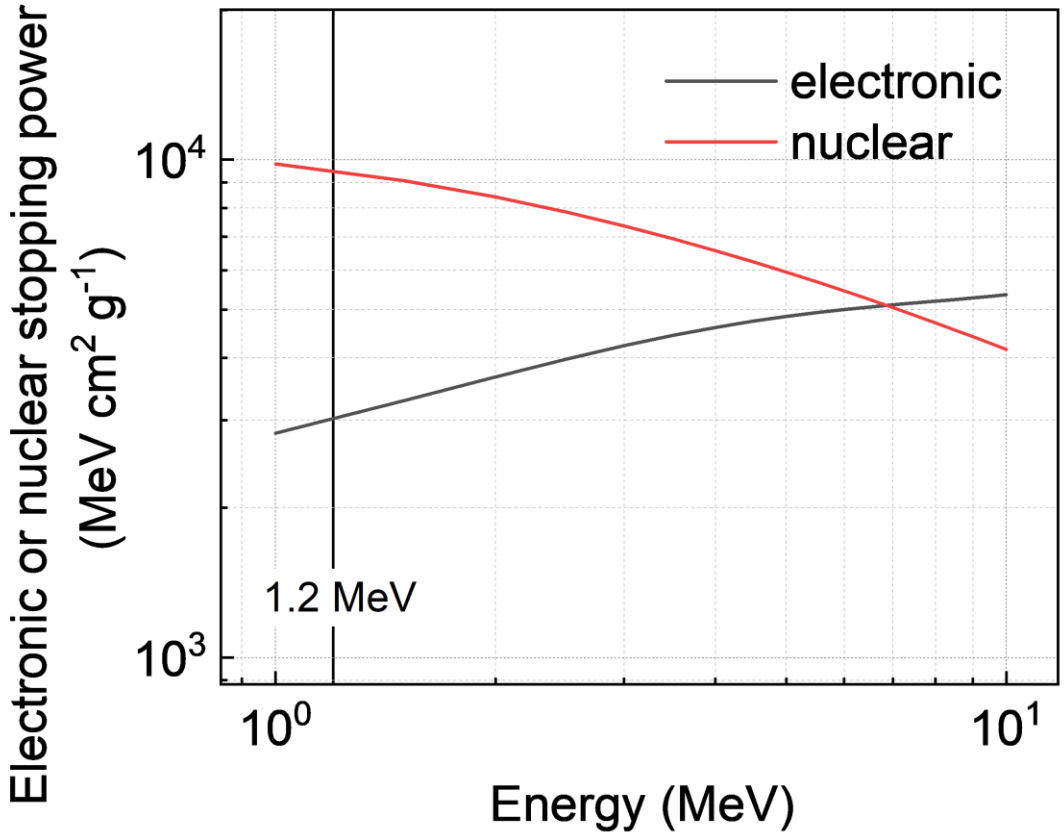

Journal of Materials Science: Materials in Electronics 34 (2023), p. 1201/1-11
https://doi.org/10.1007/s10854-023-10628-y

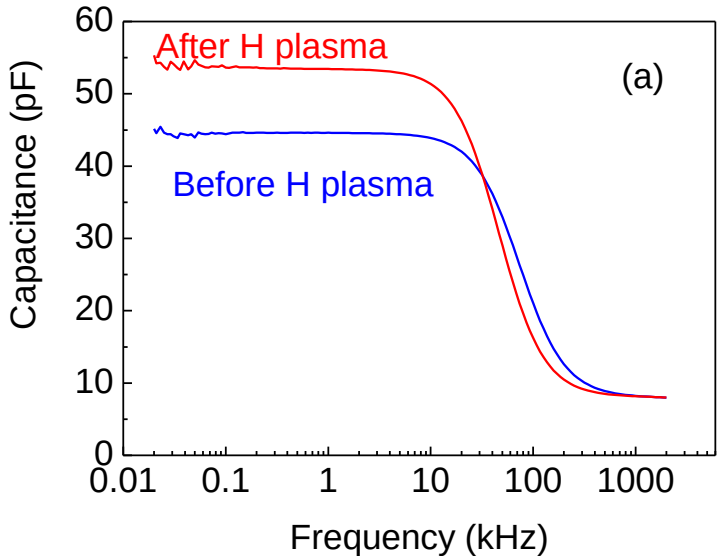

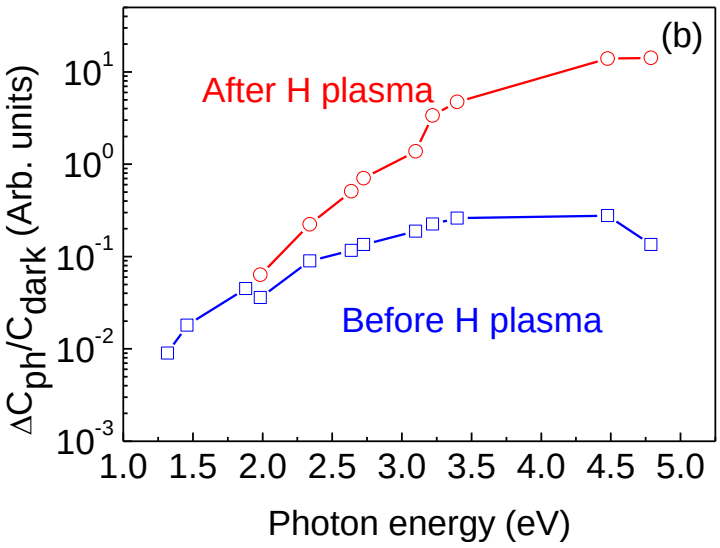

Journal of Materials Science: Materials in Electronics 34 (2023), p. 1201/1-11
https://doi.org/10.1007/s10854-023-10628-y

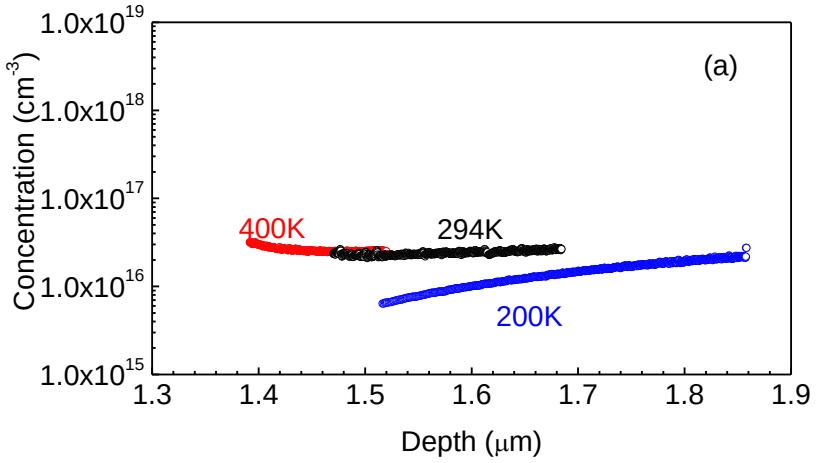

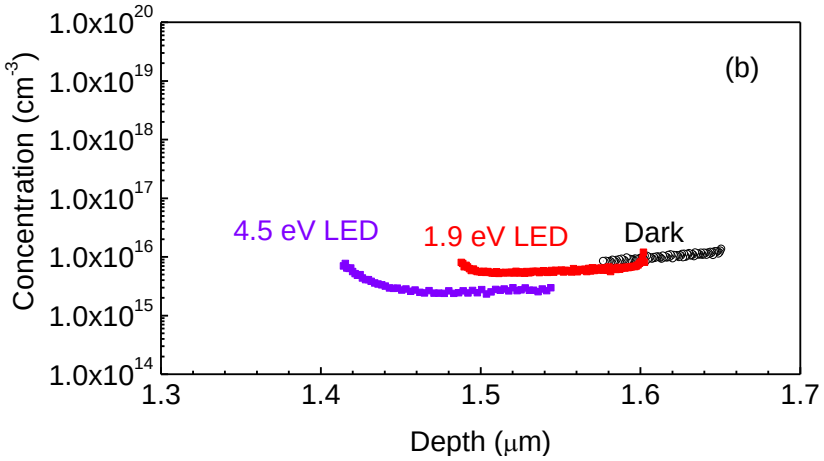

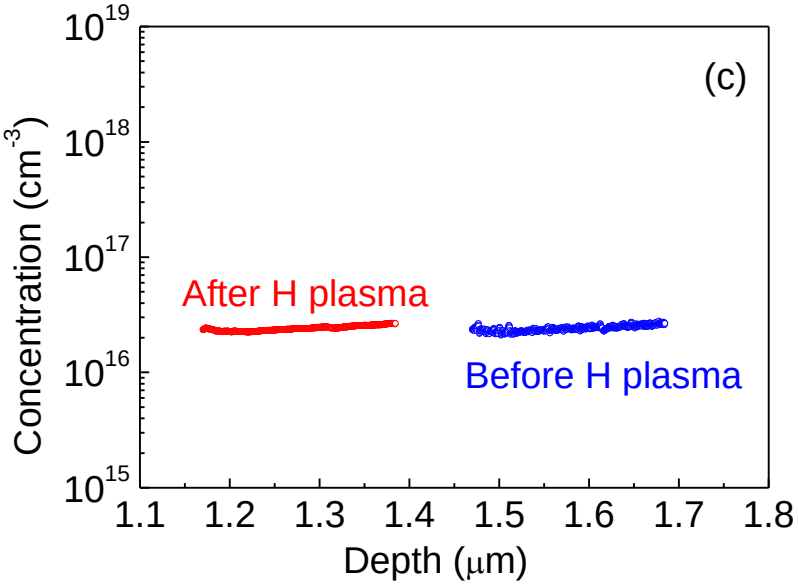

Journal of Materials Science: Materials in Electronics 34 (2023), p. 1201/1-11
https://doi.org/10.1007/s10854-023-10628-y

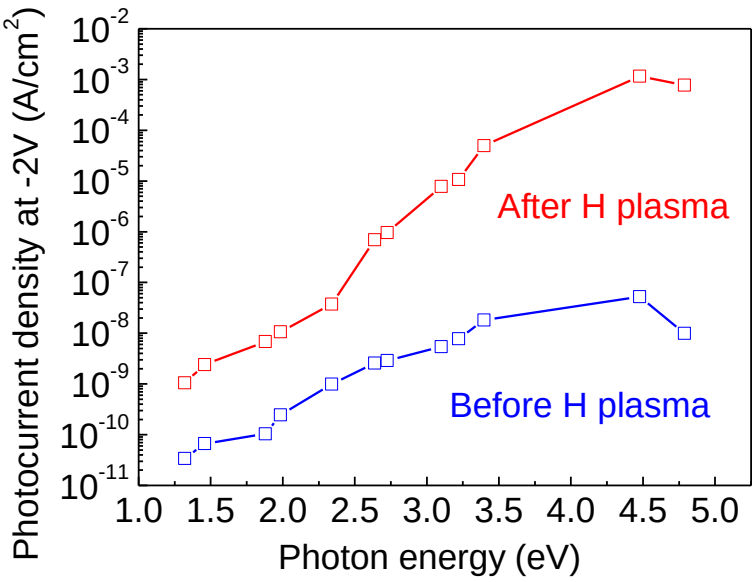

Journal of Materials Science: Materials in Electronics 34 (2023), p. 1201/1-11
https://doi.org/10.1007/s10854-023-10628-y

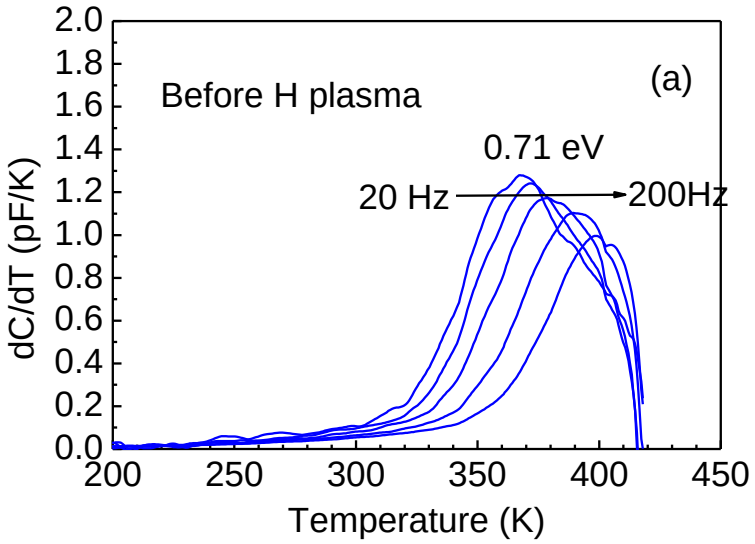

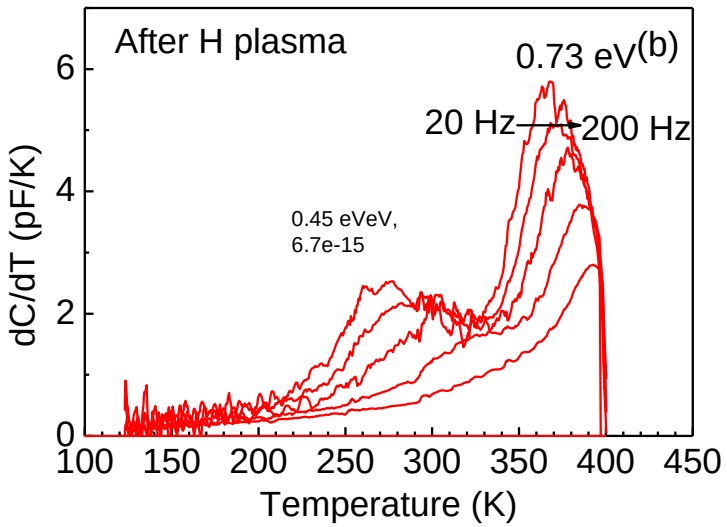

Journal of Materials Science: Materials in Electronics 34 (2023), p. 1201/1-11
https://doi.org/10.1007/s10854-023-10628-y

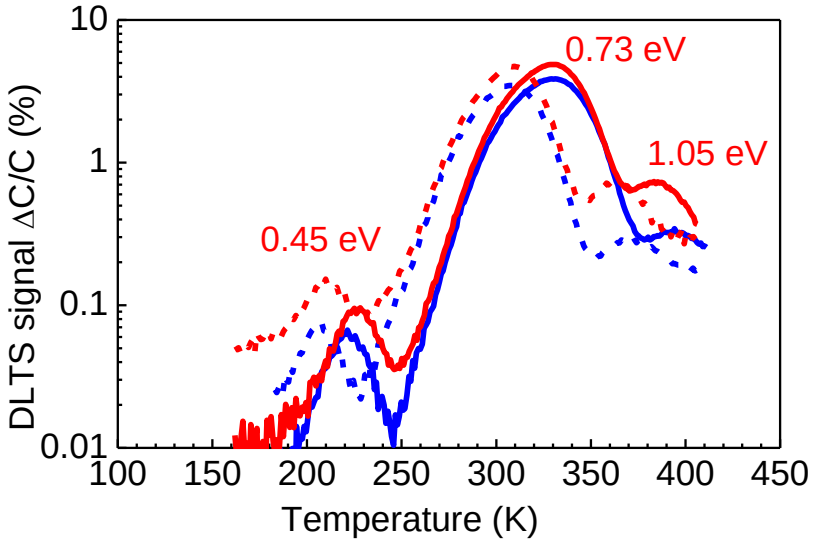

Journal of Materials Science: Materials in Electronics 34 (2023), p. 1201/1-11
https://doi.org/10.1007/s10854-023-10628-y